Secondary creep of porous metal supports for solid oxide fuel cells by a CDM approach

L. Esposito, D.N. Boccaccini, G.P. Pucillo, H.L. Frandsen

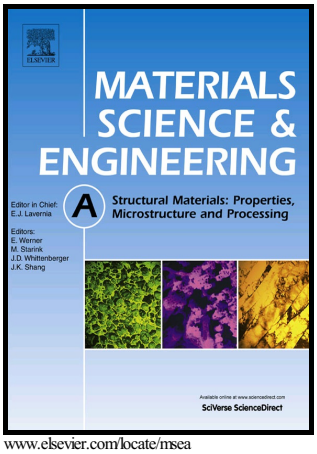

www.elsevier.com/locate/msea

PII: S0921-5093(17)30346-5
DOI: http://dx.doi.org/10.1016/j.msea.2017.03.050
Reference: MSA34833

To appear in: *Materials Science & Engineering A*

Received date: 23 February 2017
Revised date: 10 March 2017
Accepted date: 12 March 2017

Cite this article as: L. Esposito, D.N. Boccaccini, G.P. Pucillo and H.L Frandsen, Secondary creep of porous metal supports for solid oxide fuel cells b a CDM approach, *Materials Science & Engineering A* http://dx.doi.org/10.1016/j.msea.2017.03.050

Secondary creep of porous metal supports for solid oxide fuel cells by a CDM approach

L. Esposito[1*], D. N. Boccaccini[2], G.P. Pucillo[1], H. L. Frandsen[2],

[1]*Department of Industrial Engineering, University of Napoli "Federico II", P.le Tecchio 80, Napoli, 80125, Italy*

[2]*Department of Energy Conversion and Storage, Technical University of Denmark, DK-4000 Roskilde, Denmark*

**corresponding author. luca.esposito2@unina.it*

Abstract

The creep behaviour of porous iron-chromium alloy used in solid oxide fuel cells (SOFCs) becomes relevant under SOFC operating temperatures. In this paper, the secondary creep stage of infiltrated and non-infiltrated porous metal supports (MS) was investigated and theoretically modelled by a continuum damage mechanics (CDM) approach. The behaviour of the porous metal support, in the range from 1 to 17 MPa and temperatures between 650 and 700 °C, was combined and compared with data from literature of Crofer® 22 APU, taken as zero porosity reference material. The variation of the elastic modulus as function of temperature, determined by the high temperature impulse excitation technique, was directly used to account for the porosity and the related effective stress acting during the creep tests. The proposed creep rate formulation was used to extend the Crofer® 22 APU Monkman-Grant diagram in the viscous creep regime. The influence of oxide scale formation on creep behaviour of the porous MS was assessed by comparing the creep data of pre-oxidised samples tested in reducing atmosphere.

Keywords

Metal supports; creep; high-temperature ferritic stainless steel; solid oxide fuel cells

Introduction

Solid oxide fuel cells are high-temperature electrochemical devices able to convert the chemical energy of a chemical reaction directly into electric energy and heat [1]. The SOFC technology is an attractive energy conversion technology in terms of high efficiencies and fuel flexibility [1][2]. The costs and long-term stability of SOFCs are considered the primary challenges for their commercialization [2]. To enhance SOFC durability, designs of metal supported SOFC (MS-SOFC) for intermediate temperature operation have been considered [3][4][5][6][7][8][9][10]. These systems in fact offer the ductility of the metallic substrate and a higher robustness due to higher thermal conductivity compared to conventional electrode-and electrolyte-supported SOFCs [5][8]. Having an intrinsically different mechanical behaviour compared to ceramic components, metal-supported SOFCs is believed to better withstand the mechanical stresses generated by the severe vibrations and thermal gradients, when a stack is incorporated into systems used for transport applications, as APU (auxiliary power unit) and other small-scale systems [5][7][8].

Despite the promising benefits and achievements of such fuel cell, there have been some major challenges to be addressed, especially the preparation of high performance cathodes and anodes operating at lower temperatures (<700 °C) [5][7][8]. For the anode, oxidation of the porous metal substrate in the humidified hydrogen atmosphere is a problem, which would increase the anode area specific resistance due to the formation of oxide scales and the metal/oxide scale interfaces [5,11]. Another critical issue is the diffusion of metal elements like Cr, Fe, Ni between the Ni based anode and the Fe-Cr based substrate, which could inhibit the electrochemical activity of the anode, change the oxidation behaviour and the thermal expansion coefficient (CTE) of the substrate [6][12]. Despite the issues coming from the cell anode, the poor chemical compatibility and thermal expansion compatibility between the cathodes and the traditional electrolyte materials also affect the cell stability [3].

In recent years, the infiltration method has been applied to the manufacturing of MS–SOFCs to produce electrodes with high electrocatalytic activity and stability by depositing nano-sized particles into the electrode structure [13]. This method involves preparing a porous backbone, e.g. yttria-stabilized-zirconia (YSZ) backbone, sintered at a high temperature (around 1300 °C) [14], or a porous metal support [5]; then, the second component of the electrode is introduced into the porous backbone by infiltration and subsequent oxidation or reduction at a low temperature (350–850 °C) [14]. The infiltration method enables promising cell performances for the nano-structured catalysts in terms of corrosion resistance and durability [14][15]. In recent years, various perovskite structured materials have been proposed as promising fuel cell anodes for the future [16][17]. However, if preparing the electrodes by the infiltration method can circumvent the above issues, coarsening of the infiltrated nano particles is another problem [14].

The mechanical requirement of the metal support is primarily to have a good creep resistance to avoid electrolyte bending and a thermal expansion coefficient (CTE) similar to that of the electroactive ceramic components to avoid significant thermal stresses in the cell [12][18]. Even though thermal stresses do not result in failure of the metallic porous supports immediately, they may generate creep deformation and cracks in the electrolytes causing a degradation of stacks integrity and electrochemical performance under long-term operation [5][19]. Thus, primary and secondary creep behaviour of MS-SOFCs metal supports need to be experimentally characterized to predict the response of the materials under service life conditions. Secondary creep of these metal supports have previously been investigated in [12], and it was shown that simultaneous oxidation and loading resulted in significantly higher creep rates than in samples tested in an inert atmosphere or which had been exposed to pre-oxidation without load. This is similar to the effect of accelerated creep observed for ceramic supports made of Ni(O)-YSZ [20–22]. The influence of porosity have also previously been investigated by micro-structural models using re-constructed 3D geometries obtained by X-ray tomography [23][24].

In this work, we focus on the characterization of the secondary creep for the porous ferritic chromium stainless steel metal support (MS) infiltrated or not infiltrated (similar to the support described in Ref. [5]). Since the high initial porosity affects the creep material response, the behaviour of the porous MS's was compared with that of Crofer® 22 APU, taken as zero porosity reference material. The variation of the Young's modulus as function of temperature both of the MS and Crofer® 22 APU from [12] was used to adjust the nominal stress for the MS porosity. This procedure allows to compare the creep experiments carried out using a thermo mechanical analyser (TMA) [12] on porous metal support and standard creep tests on dense Crofer® 22 APU taken from literature, [25]. A unique model accounting for both diffusional and dislocational creep mechanisms was calibrated for a robustness creep life prediction on a wider stress range.

Creep modelling of the metal support

A typical creep curve (strain vs time) presents three characteristic regions [26]: I) (primary or transient creep) a period of decreasing creep rate where the resistance to creep increases until secondary stage; II) (steady state creep) a period of roughly constant creep rate, where the rate of strain-hardening is balanced by the rate of recovery; III) (tertiary creep) the fracture stage region, where there is an accelerating creep rate due to the accumulated damage related to internal void formation and/or microstructure degradation [27][28].

Although for a complete creep characterization the study of all regimes is desirable, in this work we focus on the description of the secondary creep stage since most of the SOFCs design life occurs in this phase. Since all mechanisms of steady-state creep are in some way dependent on diffusion and thermally activated processes, the dependence of creep on the absolute temperature can be described by an Arrhenius equation. Furthermore, the minimum secondary creep rate has a high dependence on stress, which is typically described by the Norton Power law [29]:

$$\dot{\varepsilon}_{ss} = A_{II}\left(\frac{\sigma}{\sigma_0}\right)^n \qquad (1)$$

where $\mathrm{A_{II}} = \mathrm{A\,e^{\left(\frac{-Q}{RT}\right)}}$ represents a temperature dependant material constant, σ is the uniaxial applied stress, *Q* the activation energy, *R* the universal gas constant, *A* is the Dorn constant, *n* is the stress exponent and σ_0 a reference stress.

Since pioneering works of Kachanov [30] and Robotnov [31], the framework of the continuum damage mechanics (CDM) has been widely used to try to predict the increase of the creep rate in the tertiary creep stage. Although the term damage is often used to implicitly indicate the formation of voids and cracks, in CDM the damage notion is much more general, since it accounts for the effects caused by all irreversible

processes, which reduce the material load carrying capability [28]. Under the assumption of isotropic damage, the damage variable is defined as,

$$D = 1 - \frac{A_{Ef}}{A_0} \tag{2}$$

where A_{Ef} and A_0 are the effective resisting area and the initial undamaged area respectively. A_{Ef} does not only account for voids, cracks and their mutual interaction, but also it accounts for initial porosity, which softens the material resistance. Since up to the minimum creep rate (secondary creep) no new voids or cracks formation is expected, damage effect on the minimum creep rate (during secondary creep) is essentially due to the porosity only. Under the strain equivalence hypothesis, the same set of constitutive equations for the dense material can still be used for the porous material simply substituting the stress with the effective stress defined as [32],

$$\tilde{\sigma} = \frac{\sigma}{1 - D} \tag{3}$$

Generally, the damage due to nucleation and growth of voids, experienced for example during large plastic deformation of a dense metal, is accounted by the material stiffness loss and is measured using the following definition, [30][33]:

$$D = 1 - \frac{E_d}{E_0} \tag{4}$$

where E_d and E_0 are the young moduli of the damaged and undamaged material, respectively. When initial porosity is relatively high, as in the case of metal foams, the stiffness decreases greatly and the simple substitution in eqn. (4) of the foam's modulus (E_f) instead of E_d, overestimate the effective stress. To overcome the problem, in this paper the estimated physical porosity at the temperatures of interest was directly assumed as the damage variable. The porosity at high temperature (and thus the damage) was linked to the dynamic Young's modulus of the foam. The term "dynamic" states a Young's modulus evaluated by the resonance frequency measurement. The resonance frequency technique is particularly suited for this scope since allows measurements in temperature and took place at very small strains, [34].

Several models to correlate the elastic modulus of the foam (E_f) with the porosity (ϕ) are available, [35]. The nonlinear semi-empirical formulation proposed by Phani and Niyogi [36], $E_f = E_0(1 - \phi/\alpha)^\beta$, was selected, where α and β are constants to identify.

Assuming the physical porosity approximately equal to the damage, the following operative non-evolutive definition of the initial damage due to the porosity is achieved:

$$D_0 = \alpha \cdot \left[1 - \left(\frac{E_f}{E_0} \right)^{\frac{1}{\beta}} \right] \tag{5}$$

where E_f and E_0 are the dynamic young moduli of the foam and dense material, respectively.

Hardin and Beckermann, [24], by measurements on cast steels, found 0.5 and 2.5 for α and β respectively. However, the less than unity hypothesis for the "α" value introduces a critical porosity that reduces up to α the range of variability for damage. Since damage variable ranges between 0 and 1 the α value was assumed equal to 1 and β was estimated equal to 6 in order to have agreement with the Hardin and Beckermann formulation up to 30% of porosity.

The effective stress provides a driving force for dislocation movement and diffusion of atoms. Thus, as the stress is increased, the rate of deformation also increases. Prediction of the power "*n*" value of eqn. (1) from first principles is not easy, as its value depends on which mechanism of creep is operating. For example, for diffusion creep "*n*" value is approximately 1, while for dislocation creep it is usually varying from metal to metal in the range 3-8 (the most common value is "*n*" =5). The activation energy, *Q*, is determined experimentally from the slope of a plot of the natural logarithm of creep rate against the reciprocal of temperature. Bonora et al. [37], proposed a mechanisms based model to account for the minimum creep rate over wide stress range in dislocational regime. Recently, Esposito et al. [38] extended that model to account for transition from the viscous to the dislocational regime. This latter formulation is shown in eqn. (6) and is adopted in this work using the effective stress for porous metal supports.

$$\dot{\varepsilon}_m = A_0 \exp\left(-\frac{Q^{\perp}}{RT}\right)\left(\frac{\tilde{\sigma}-\sigma_{th}^{\perp}}{\sigma_0}\right)^{\exp\left[\left(\frac{\sigma}{\sigma_0}\right)^m\right]} + B_0 \exp\left(-\frac{Q^d}{RT}\right)\left(\frac{\tilde{\sigma}}{\sigma_0}\right) \quad (5)$$

The minimum creep rate in eqn. (6) is predicted by the sum of two terms: the first account for dislocational processes and the second for diffusive strain accumulation (leading at lower stresses). A different activation energy, $Q^{\perp}$ and Q^d for dislocational and diffusional regimes respectively, determines the temperature dependency of the two types of creep mechanisms. A threshold stress, $\sigma_{th}^{\perp}$, below which the dislocation motion is inhibited due to the lattice drag resistance, is also considered.

Materials and sample preparation

The mechanical experiments were performed on the commercially available dense ferritic steel Crofer® 22 APU (Crofer) and porous ferritic steel alloys (MS) fabricated in-house at Technical University of Denmark. The fabrication of the MSs was reported in details elsewhere [5]. The chemical composition of Crofer and MS is similarly composed of ~22 wt.% of chromium with ~0.5 wt.% of Mn and with some other minor elements (La,Ti) balanced by iron, [39]. The porosity of MS at room temperature was determined by mercury intrusion (Micromeritics' Autopore IV 9500V1.05). The resulting porosity of MS was about 18%. The experiments were performed on infiltrated and non-infiltrated MSs.

Infiltration of electrocatalysts

Some samples were subjected to infiltration process as described in ref. [39]. These samples will be hereafter called MSI. Briefly, aqueous precursors solution of various nitrate salts (Ce, Gd, Ni nitrate) were prepared by mixing stoichiometric and calibrated amounts of precursors together with a suitable surfactant. The concentration of cations in the solution was normally fixed at 0.03mole/10gH_2O. After infiltration, the cells were calcinatated at 350°C in air for two hours. The infiltration procedure ensured a uniform coating of nano-sized particles on all the surfaces of the backbone structure (including the metal support in the half-cells). A SEM image of a metal support and the infiltrated phase is shown in Figure 1. The amount (wt.%) of infiltrated material in the porous electrodes was estimated by weighing the cells before and after infiltration and calcination and subtracting the approximate weight of the electrolyte. The most promising infiltration solution had the composition $Ce_{0.8}Gd_{0.2}O_{1.9}$ + 10wt% Ni (called Ni:CGO). This above specified infiltration solution has been used in all the test cells here investigated. The effectiveness of the infiltration solution was based on electrochemical performance as a fuel electrode in symmetrical cell tests [39].

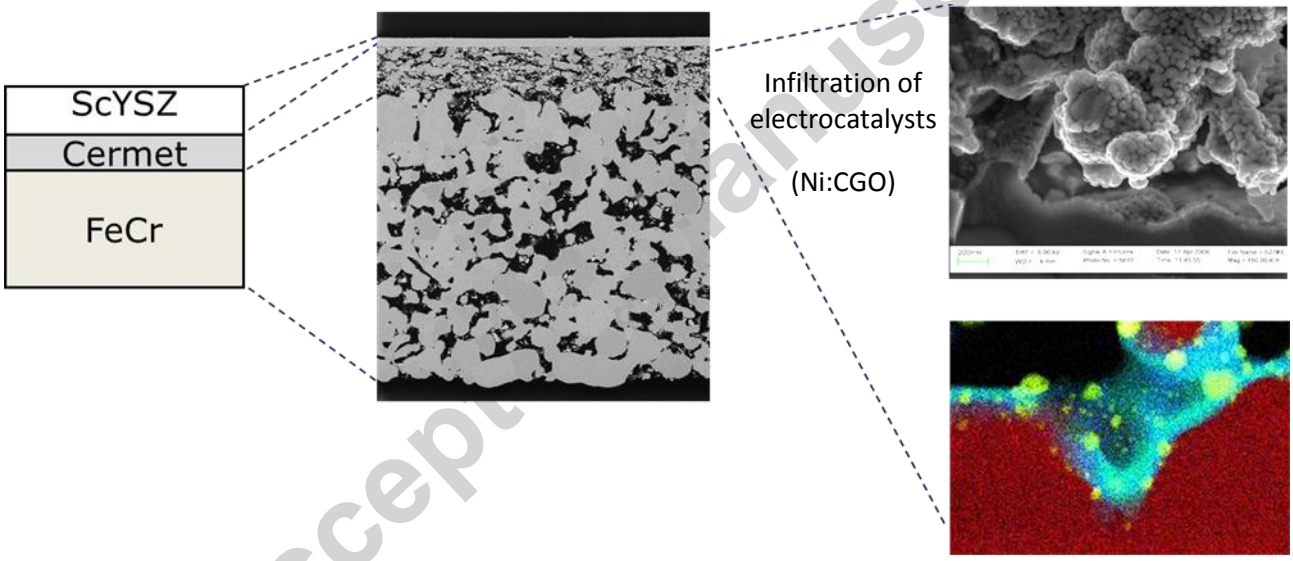

Figure 1: Schematic illustration together with a SEM image showing the concept of the metal supported cell design and the infiltration of electrocatalysts (Ni:CGO)

Young's modulus of metal supports by high temperature impulse excitation technique

The Young's modulus was calculated accordingly to the ASTM E 1876-99 standard by impulse excitation of vibration, [41]. For high temperature impulse excitation technique (HT-IET) the samples were laser cut with dimensions of (15 ± 1)mm x (0.3 ± 0.01)mm x (0.5 ± 0.01)mm from both dense Crofer sheets and sintered porous MS. The MS and Crofer samples were laser cut perpendicular to the tape casting and cold rolling, respectively. The rectangular samples were suspended in the nodes of their first bending vibration mode with platinum-rhodium threads, and positioned in the HT-IET-furnace (HT1600, IMCE, Genk, Belgium). The

samples were subsequently subjected to a thermal cycle from room temperature to 700 °C with a heating and cooling rate of 5 °C/min and a dwell time of 2 h at 700°C. The samples were excited periodically by the impact of a small ceramic projectile. The resonant flexural frequencies of vibration are deduced from the recorded digitized sound signal by Fast Fourier Transform (FFT). When the fundamental resonant frequency (f_f), as well as the mass (m) and the dimensions of the sample are accurately known, the Young's modulus can be calculated as [40]:

$$E = 0.9465 \frac{m f_f^2 l^3}{b d^3} T_1 \quad (6)$$

where b, l and d, are the width, length and thickness of the bar respectively and T1 a correction factor depending on the thickness-to-length ratio and Poisson ratio of the material. Since the thickness-to-length ratio considered here was small the value of T1 was set to 1. The HT-IET experiments were performed in air.

In Figure 2a the Young's moduli from [12] averaged over the temperature are shown. The evolution with the temperature of the Young's moduli ratio and the porosity damage calculated by the eqn. (5) is shown in Figure 2b). The porosity damage "D_0" increases slightly with the increase of the temperature ranging from 0.201 at room temperature up to 0.236 at 700 °C.

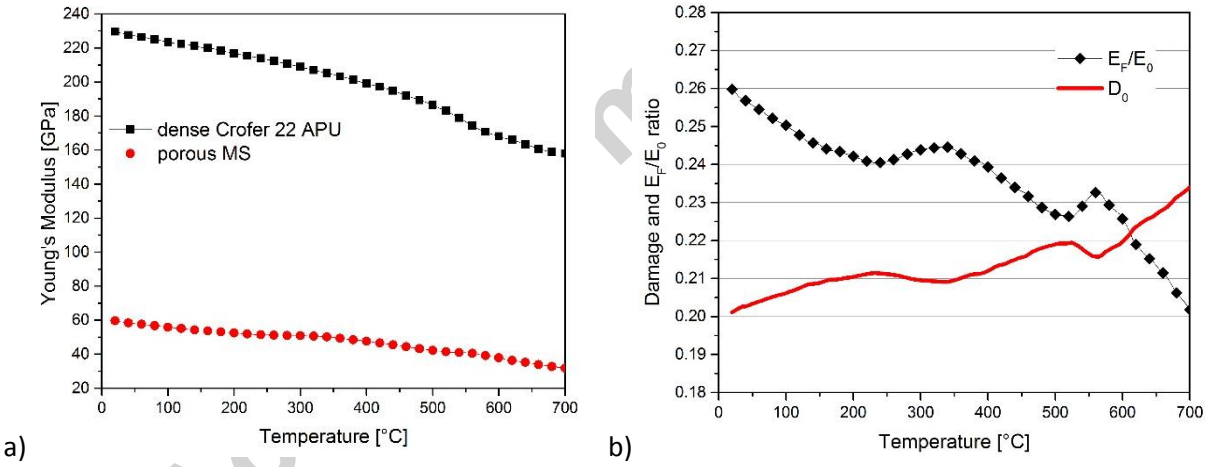

Figure 2: a) Young's modulus as a function of temperature of porous MS and Crofer tested in air; b) Initial damage related to the porosity evaluated by Young moduli ratio

Creep experiments

The creep rate of the porous metal samples was measured for nominal stresses in the range from 1 to 17 MPa [12] by uniaxial tension using thermo-mechanical analysis (TMA) (NETZSCH, TMA 402 F1 Hyperion®). Dimensions of (60 ± 1) mm x (0.3 ± 0.01) mm x (10 ± 1) mm were used for MS creep testing. Each specimen was held at the specified temperature for 15 minutes prior to applying the load. Since the

oxidizing environment (responsible for the presence of oxide scales formed during creep testing) can affect the strain rate of the porous metals, additional creep tests in a reducing atmosphere on MSI and pre-oxidised samples were performed. The creep strain-time curves at various temperatures were then obtained from these experiments and the creep model parameters deduced. The creep data of Crofer® 22 APU on a more extended stress range (8 - 100 MPa) using a traditional lever arm machine, were collected from literature [25].

Creep rate and modelling results

In order to compare creep rate of porous metal support and dense Crofer, the nominal stress used for MS creep testing was converted in effective stress using eqn. (3) and the damage values reported in Figure 2b). The minimum creep rates of MS and Crofer are plotted in figure 3 and figure 4 for 650 and 700°C respectively. The changes of the linearity of Norton plots are related to changes in the creep mechanism for the materials, [1] [37]. Porous MS in air at 650 and 700°C exhibits a linear trend in the stress regime between 3-12MPa. This suggests that no changes in the creep mechanism of the investigated samples occur in this stress range. This is particularly the case at 650°C, where the exponent *n* is close to 1 and slightly higher at 700°C, typical values for diffusional regime. However, for applied stresses higher than 12-15 MPa a change in the creep mechanism as described by Khun [41] for Crofer is apparent, as *n* exponent increases. Chiu et al. [25] found *n* value ranging from 5 to 6 on contiguous but higher stress range for Crofer® 22 APU.

As shown in Figure 3 and Figure 4, where dense Crofer and MS data are plotted together, both datasets have a common trend. However, the *n* value tends to increase for larger stress levels the Crofer 22 APU. This points towards the inadequacy of the Norton formulation on the entire stress range due to the transition between creep mechanisms (viscous to the dislocational), why there is a need to apply the more complex creep model in eqn. (6).

With the highest stress levels and most distant from the stress linearity (*n=1*), the Crofer data were assumed most affected by dislocational processes and used to calibrate the first term of eqn. (6). For the same dataset Chiu et al. [25] found a slight stress dependent activation energy with an average value of 393 KJ/mol. That value was used here as $Q^{\perp}$ to normalize the minimum creep rate on temperature from 650 to 800°C. The normalized creep rate, $\dot{\varepsilon}_m \cdot \exp\left(Q^{\perp}/RT\right)$, as function of the applied stress is shown in Figure 5.

The best fitting of the dislocational data using both the non-linear formulation and the Norton law is reported. Although, a good approximation can be achieved by the Norton law (with *n*=5.72), the correlation coefficient R^2 give a more quantitative evidence of the better fitting when the proposed non-linear model is used.

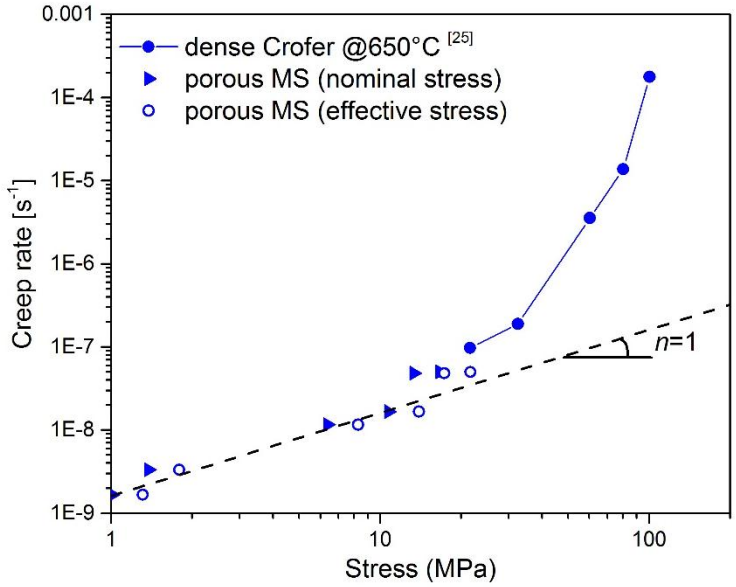

Figure 3: Comparison of MS minimum creep rate plotted versus the effective stress and nominal stress together with Crofer data at 650°C

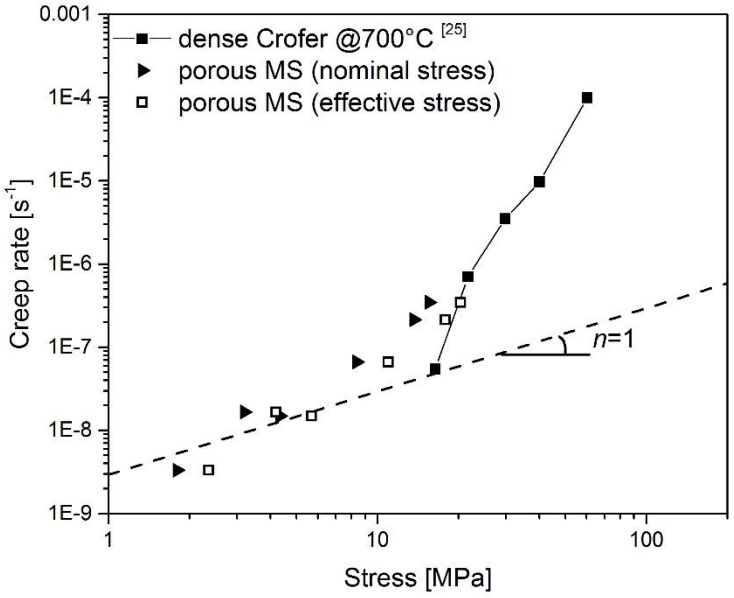

Figure 4: Comparison of MS minimum creep rate plotted versus the effective stress and nominal stress together with Crofer data at 700°C

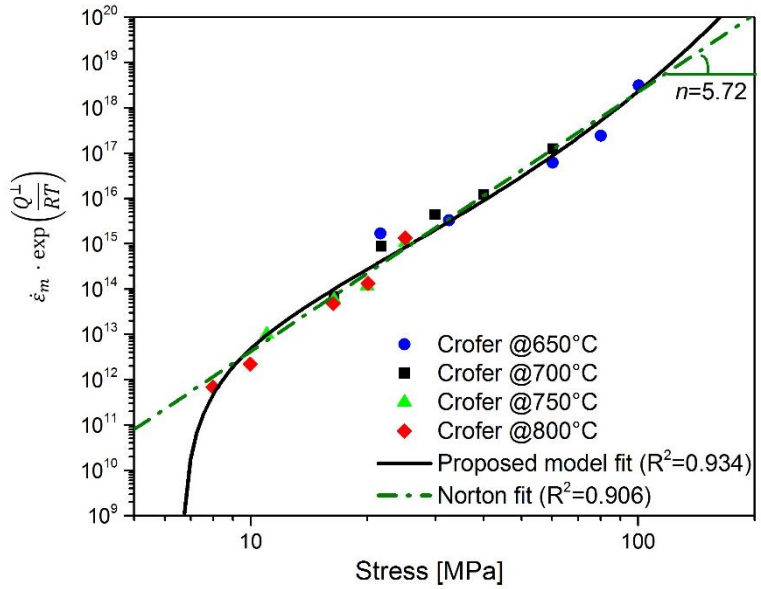

Figure 5: Crofer creep rate form Chiu et al. [25] normalized by the Arrhenius term and interpolated by the proposed model

The MS creep rates at lower stresses, under the assumption of purely viscous creep mechanism, were used to identify B_0 and Q^d by interpolation on the effective stress corrected data. The identified parameters merging dense Crofer and porous MS data, are summarized in table 1. In Figure 6 the capability of the proposed model to predict the creep rate for different stresses and temperatures is shown. It is worth to remark that longer duration test of porous MS in air could be more scattered as effect of the oxide scale formation. The relatively low value found for Q^d could be also due to this effect.

The model sensitivity to the initial damage variations was checked comparing the creep rate predictions for different damage values. In Figure 7 the effect of the initial damage on the predicted creep rate at 650°C is shown.

Table 1: Model parameters for Crofer 22 APU

A_0 [h^{-1}]	$Q^{\perp}$ [J/mol]	$\sigma_{th}^{\perp}$ [MPa]	m	σ_0 [MPa]	B_0 [h^{-1}]	Q^d [J/mol]
5.3635e+13	393000	6.6	0.152	8.0	1.6e-3	90000

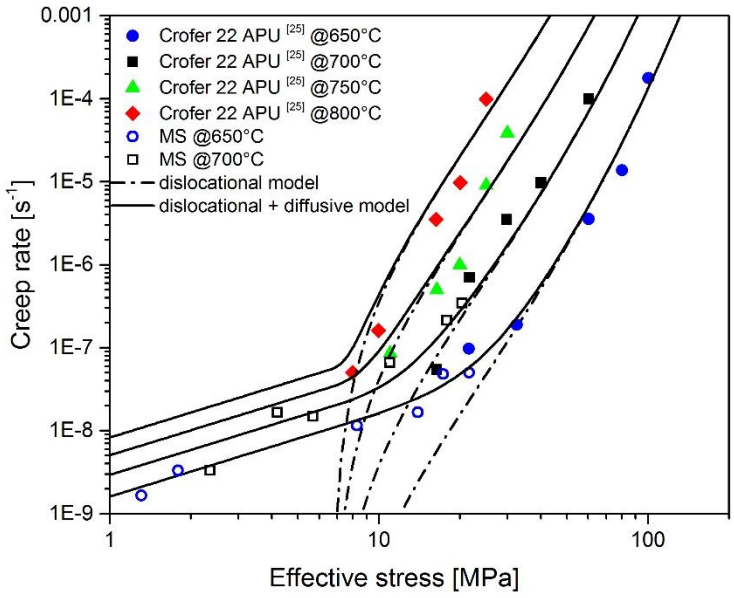

Figure 6: Transferability in stress and temperature of the proposed model

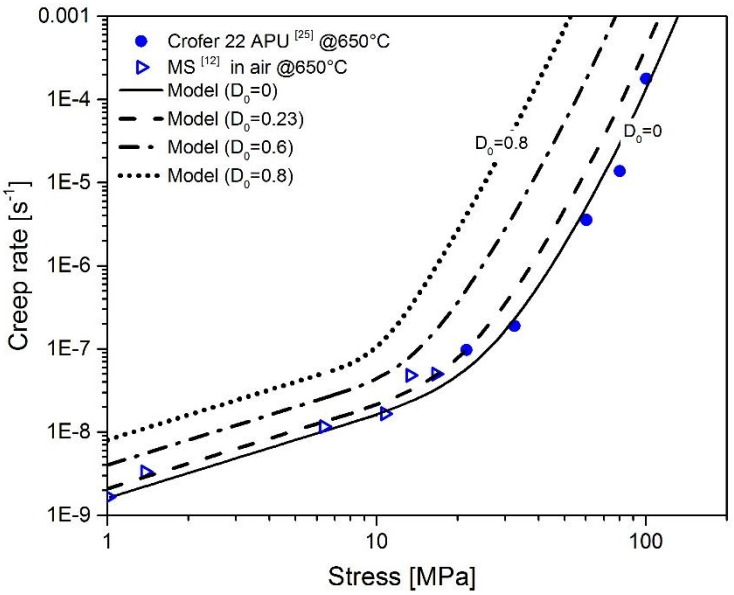

Figure 7: Effect of the initial damage (≈porosity) on the creep rate at 650°C

Effect of infiltration and oxide scale formation on the creep rate

Creep experiments were also performed on the infiltrated samples (MSI) to investigate if the transition between the creep regimes also could be observed for these. Furthermore, some of the infiltrated samples prepared for creep testing were exposed to 850 °C in $Ar/H_2O/H_2$ atmosphere (pH_2O/pH_2 = 9) in 2, 10 and 250 h to investigate the influence of oxide scales on the creep behaviour. These samples are hereafter called MSI-2h, MSI-10h and MSI-250h, respectively. The creep tests on pre-oxidised and non-oxidised samples were carried out in a reducing atmosphere to limit further scale growth during the test. The

reducing atmosphere was composed by 9% hydrogen in nitrogen ($10^{-24} < pO_2 < 10^{-12}$ atm, from hereafter written as 9% H_2).

In Figure 8, the comparison of the obtained creep rates is shown. The infiltration seems to have a negligible effect on the creep rate when comparing to the non-infiltrated samples. The oxide formation however affects the creep strain rate significantly. The creep rates are lower in presence of oxide scale formation and decrease for longer pre-oxidation time. Generally, the creep rate is expected higher as effect of the oxidation processes, [42], (according to the authors' knowledge this statement has not previously been verified for porous metals in diffusive stress regime), but in this study a different trend is now recognized.

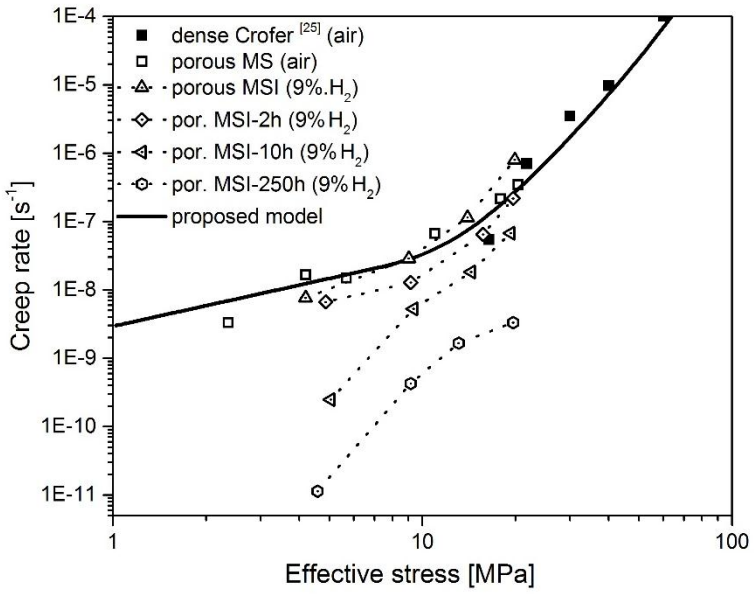

Figure 8: Effect of infiltration and pre-oxidation on creep rate of metal support at 700°C

Monkman-Grant diagram for Crofer 22 APU

The well-known Monkman-Grant (M-G) relationship [43] is primarily used to estimate the time to failure by the minimum creep rate of the material. The Monkman-Grant diagram shows the rupture stress versus the time to rupture, t_r, and thus the M-G curves are commonly used for creep strength assessment and also to compare the creep performance of different materials. Since creep rupture is ruled by several evolution damage processes and by stress triaxiality, [44], the times to failure of porous MS and dense Crofer are not comparable, while a good correlation among minimum creep-rates was found. Consequently, the effective stresses and minimum creep-rates of porous MS were used to extend the M-G diagram for dense Crofer in viscous creep regime. The time to rupture was evaluated as,

$$t_r = \frac{M}{\dot{\varepsilon}_m} \tag{7}$$

where the calibrated formulation given in Eqn. (6) is used for $\dot{\varepsilon}_m$ to ensure the transferability in stress and temperature. The constant *M* was assumed equal to 1.886e-4 which is the mean value of the products $t_r \cdot \dot{\varepsilon}_m$ from the experimental data of Chiu et al. [25]. In Figure 9, the extended M-G diagram for Crofer is shown. The non-linearity of the model (continuous lines), in agreement with experimental data (scatter points), is achieved by the accuracy of the proposed model for minimum creep rate. There are no experimental results for time to rupture at low stresses, as this involves very long experiments. Thus, in lack of such the steep part of the G-M diagrams, relating to the diffusional creep, should be considered as a proposal based on the observed creep behaviour.

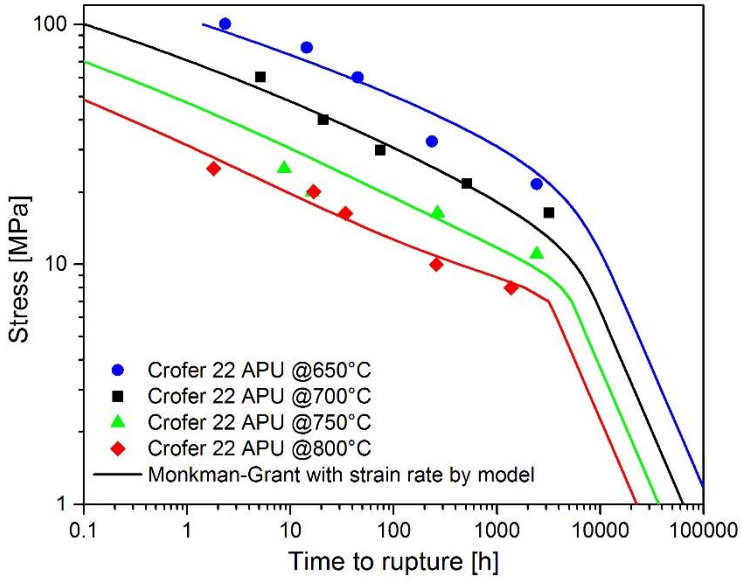

Figure 9: Monkman-Grant diagram for Crofer extended in viscous regime

Conclusion

In this work a creep model which can embrace the various experimental results on creep of Crofer 22 APU and porous metal supports in the literature, to achieve more reliable thermo-mechanical predictions and hereby increase the robustness of the SOFC technology, was proposed. The relationship between minimum creep rate of porous metal supports and dense Crofer 22 APU was investigated and a mechanisms based approach, accounting for porosity, was used to analyse the results. Main paper outcomes are summarized as follows:

a) The stress exponent of the porous metal support was found to be close to the value obtained for the dense Crofer 22 APU, when the same stress and atmosphere condition is considered.

b) For higher stress levels a change of the creep deformation mechanism is evident for Crofer 22 APU. At low stress, diffusion mechanism dominates resulting in a rate equation with a

creep exponent *n* close to 1. At higher stress levels a presence of a sharp change of slope in the Norton plot is observed indicating dislocational creep. However, a model accounting for both diffusional creep and dislocational creep can be used to embrace the different experimental results.

c) The metal supports tested in oxidizing atmosphere show the highest strain rates, while the pre-oxidized samples showed the lowest strain rates. Based on this, it could be stated that scale formation during creep testing or the presence of thick oxide scale layer before testing (pre-oxidation treatment) affect significantly the creep behaviour of the porous materials.

d) The time to rupture for Crofer 22 APU was estimated combining the proposed calibrated model with the Monkman-Grant law. Hereby it is possible to estimate the time to rupture in diffusional creep regime at very low stresses.

References

[1] S.M. Haile, Fuel cell materials and components, Acta Mater. 51 (2003) 5981–6000. doi:10.1016/j.actamat.2003.08.004.

[2] K. Kendall, M. Kendall, High-Temperature Solid Oxide Fuel Cells for the 21st Century, 2016. doi:10.1016/B978-0-12-410453-2.09994-2.

[3] T. Klemensø, J. Nielsen, P. Blennow, Å.H. Persson, T. Stegk, B.H. Christensen, S. Sønderby, High performance metal-supported solid oxide fuel cells with Gd-doped ceria barrier layers, J. Power Sources. 196 (2011) 9459–9466. doi:10.1016/j.jpowsour.2011.07.014.

[4] Y.-T. Chiu, C.-K. Lin, High-Temperature Stress-Rupture Properties of a Ferritic Steel for Solid Oxide Fuel Cell Interconnect, in: ECS Trans., The Electrochemical Society, 2011: pp. 2581–2590. doi:10.1149/1.3570257.

[5] P. Blennow, J. Hjelm, T. Klemensø, S. Ramousse, A. Kromp, A. Leonide, A. Weber, Manufacturing and characterization of metal-supported solid oxide fuel cells, J. Power Sources. 196 (2011) 7117–7125. doi:10.1016/j.jpowsour.2010.08.088.

[6] J.A. Glasscock, L. Mikkelsen, Å.H. Persson, G. Pećanac, J. Malzbender, P. Blennow, F. Bozza, P. V. Hendriksen, Porous Fe21Cr7Al1Mo0.5Y metal supports for oxygen transport membranes: Thermo-mechanical properties, sintering and corrosion behaviour, Solid State Ionics. 242 (2013) 33–44. doi:10.1016/j.ssi.2013.04.006.

[7] C. Metcalfe, J. Harris, J. Kuhn, M. Marr, O. Kesler, Progress in Metal-Supported Axial-Injection Plasma Sprayed Solid Oxide Fuel Cells Using Nanostructured NiO-Y0.15Zr0.85O1.925 Dry Powder Anode Feedstock, J. Therm. Spray Technol. 22 (2013) 599–608. doi:10.1007/s11666-013-9884-0.

[8] M.C. Tucker, Progress in metal-supported solid oxide fuel cells: A review, J. Power Sources. 195 (2010) 4570–4582. doi:10.1016/j.jpowsour.2010.02.035.

[9] S. Linderoth, Solid oxide cell R&D at Risø National Laboratory—and its transfer to technology, J. Electroceramics. 22 (2009) 61–66. doi:10.1007/s10832-008-9458-6.

[10] B.J. McKenna, N. Christiansen, R. Schauperl, P. Prenninger, J. Nielsen, P. Blennow, T.

Klemensø, S. Ramousse, A. Kromp, A. Weber, Advances in Metal Supported Cells in the METSOFC EU Consortium, Fuel Cells. 13 (2013) 592–597. doi:10.1002/fuce.201200185.

[11] G. Reiss, H.L. Frandsen, Å.H. Persson, C. Weiß, W. Brandstätter, Numerical evaluation of oxide growth in metallic support microstructures of Solid Oxide Fuel Cells and its influence on mass transport, J. Power Sources. 297 (2015) 388–399. doi:10.1016/j.jpowsour.2015.08.020.

[12] D.N. Boccaccini, H.L. Frandsen, B.R. Sudireddy, P. Blennow, Å.H. Persson, K. Kwok, P. Vang Hendriksen, Creep behaviour of porous metal supports for solid oxide fuel cells, Int. J. Hydrogen Energy. 39 (2014) 21569–21580. doi:10.1016/j.ijhydene.2014.07.138.

[13] R.P. Dowd, S. Lee, Y. Fan, K. Gerdes, Engineering the solid oxide fuel cell electrocatalyst infiltration technique for industrial use, Int. J. Hydrogen Energy. 41 (2016) 14971–14981. doi:10.1016/j.ijhydene.2016.06.015.

[14] T. Klemensø, D. Boccaccini, K. Brodersen, H.L. Frandsen, P. V. Hendriksen, Development of a novel ceramic support layer for planar solid oxide cells, Fuel Cells. 14 (2014) 153–161. doi:10.1002/fuce.201300121.

[15] M. Etaat, H. Pouraliakbar, G. Khalaj, M. Ghambari, Adhesion strength measurement of nickel layer on the iron-based P/M parts influenced by different surface pre-treatment operations, Measurement. 66 (2015) 204–211. doi:http://dx.doi.org/10.1016/j.measurement.2015.02.006.

[16] A. Atkinson, S. Barnett, R.J. Gorte, J.T.S. Irvine, a J. McEvoy, M. Mogensen, S.C. Singhal, J. Vohs, Advanced anodes for high-temperature fuel cells., Nat. Mater. 3 (2004) 17–27. doi:10.1038/nmat1040.

[17] B.A. Boukamp, Fuel cells: The amazing perovskite anode., Nat. Mater. 2 (2003) 294–296. doi:10.1038/nmat892.

[18] L. Niewolak, F. Tietz, W.J. Quadakkers, Interconnects, in: K. Kendall, M. Kendall (Eds.), High Temp. Solid Oxide Fuel Cells 21st Century, Academic Press, 2015: p. 520.

[19] A. Nakajo, J. Kuebler, A. Faes, U.F. Vogt, H.J. Schindler, L.-K. Chiang, S. Modena, J. Van herle, T. Hocker, Compilation of mechanical properties for the structural analysis of solid oxide fuel cell stacks. Constitutive materials of anode-supported cells, Ceram. Int. 38 (2012) 3907–3927. doi:10.1016/j.ceramint.2012.01.043.

[20] H.L. Frandsen, M. Makowska, C. Chatzichristodoulou, F. Greco, D.W. Ni, D.J. Curran, M. Strobl, L. Theil Kuhn, P.V. Hendriksen, Accelerated creep in solid oxide fuel cell anode supports during reduction, J. Power Sources. 323 (2016) 78–89.

[21] M.G. Makowska, M. Strobl, E.M. Lauridsen, S. Kabra, W. Kockelmann, A. Tremsin, H.L. Frandsen, L. Theil Kuhn, *In situ* time-of-flight neutron imaging of NiO–YSZ anode support reduction under influence of stress, J. Appl. Crystallogr. 49 (2016) 1674–1681. doi:10.1107/S1600576716012668.

[22] M.G. Makowska, L.T. Kuhn, H.L. Frandsen, E.M. Lauridsen, S. De Angelis, L.N. Cleemann, M. Morgano, P. Trtik, M. Strobl, Coupling between creep and redox behavior in nickel - yttria stabilized zirconia observed in-situ by monochromatic neutron imaging, J. Power Sources. 340 (2017) 167–175. doi:10.1016/j.jpowsour.2016.11.059.

[23] K. Kwok, D. Boccaccini, Å.H. Persson, H.L. Frandsen, Homogenization of steady-state creep of porous metals using three-dimensional microstructural reconstructions, Int. J. Solids Struct. 78–79 (2016) 38–46. doi:10.1016/j.ijsolstr.2015.09.020.

[24] R.A. Hardin, C. Beckermann, Effect of Porosity on the Stiffness of Cast Steel, Metall. Mater. Trans. A. 38 (2007) 2992–3006. doi:10.1007/s11661-007-9390-4.

[25] Y.-T. Chiu, C.-K. Lin, J.-C. Wu, High-temperature tensile and creep properties of a ferritic stainless steel for interconnect in solid oxide fuel cell, J. Power Sources. 196 (2011) 2005–

2012. doi:10.1016/j.jpowsour.2010.09.083.
[26] M.E.K. and M.-T. Pérez-Prado, Fundamentals of Creep in Metals and Alloys, 2nd Editio, Elsevier Ltd, 2004.
[27] B. Wilshire, H. Burt, Damage evolution during creep of steels, Int. J. Press. Vessel. Pip. 85 (2008) 47–54. doi:10.1016/j.ijpvp.2007.06.002.
[28] L. Esposito, N. Bonora, Time-independent formulation for creep damage modeling in metals based on void and crack evolution, Mater. Sci. Eng. A. 510–511 (2009). doi:10.1016/j.msea.2008.06.052.
[29] F.H. Norton, The creep of steel at high temperatures, McGraw-Hill, New York, 1929.
[30] L.M. Kachanov, Time of the rupture process under creep conditions, Izv. Akad. Nauk. S.S.R. Otd. Tekh. Nauk. 8 (1958).
[31] Y.N. Rabotnov, Creep problems in structural members., North-Holland, Amsterdam, 1969.
[32] J. Lemaitre, A course on damage mechanics, Springer-Verlag, Berlin, New York, 1992.
[33] N. Bonora, A. Ruggiero, S. De Meo, D. Gentile, L. Esposito, A revised approach to damage measurement based on stiffness loss technique, in: Proc. PVP2008, 2008: pp. 1–5. doi:10.1115/PVP2008-61035.
[34] O. Friedl, C. Motz, H. Peterlik, S. Puchegger, N. Reger, R. Pippan, Experimental Investigation of Mechanical Properties of Metallic Hollow Sphere Structures, Metall. Mater. Trans. B. 39 (2008) 135–146. doi:10.1007/s11663-007-9098-2.
[35] J.-F. Despois, R. Mueller, A. Mortensen, Uniaxial deformation of microcellular metals, Acta Mater. 54 (2006) 4129–4142. doi:10.1016/j.actamat.2006.03.054.
[36] K.K. Phani, S.K. Niyogi, Young's modulus of porous brittle solids, J. Mater. Sci. 22 (1987) 257–263. doi:10.1007/BF01160581.
[37] N. Bonora, L. Esposito, Mechanism based creep model incorporating damage, J. Eng. Mater. Technol. Trans. ASME. 132 (2010). doi:10.1115/1.4000822.
[38] L. Esposito, N. Bonora, G. De Vita, Creep modelling of 316H stainless steel over a wide range of stress, in: Procedia Struct. Integr., 2016: pp. 927–933. doi:10.1016/j.prostr.2016.06.119.
[39] P. Blennow, J. Hjelm, T. Klemensø, Å.H. Persson, S. Ramousse, M. Mogensen, Planar Metal-Supported SOFC with Novel Cermet Anode, Fuel Cells. 11 (2011) 661–668. doi:10.1002/fuce.201100029.
[40] ASTM E 1876–99, Standard Test method for Dynamic Young's Modulus, Shear Modulus and Poisson's Ratio by Impulse Excitation of Vibration. 2000, ASTM Committee E-28 on Mechanical Testing, subcommittee E2803 on Elastic Properties., (n.d.).
[41] B. Kuhn, C.A. Jimenez, L. Niewolak, T. Hüttel, T. Beck, H. Hattendorf, L. Singheiser, W.J. Quadakkers, Effect of Laves phase strengthening on the mechanical properties of high Cr ferritic steels for solid oxide fuel cell interconnect application, Mater. Sci. Eng. A. 528 (2011) 5888–5899. doi:10.1016/j.msea.2011.03.112.
[42] C. Asensio-Jimenez, L. Niewolak, H. Hattendorf, B. Kuhn, P. Huczkowski, L. Singheiser, W.J. Quadakkers, Effect of Specimen Thickness on the Oxidation Rate of High Chromium Ferritic Steels: The Significance of Intrinsic Alloy Creep Strength, Oxid. Met. 79 (2012) 15–28. doi:10.1007/s11085-012-9323-5.
[43] F.C. Monkman, N.J. Grant, An empirical relationship between creep rupture life and minimum creep rate in creep rupture tests, in: Am. Soc. Testings Mater., 1956: pp. 593–607.
[44] N. Bonora, L. Esposito, S. Dichiaro, Predicting creep rupture using damage mechanics, in: Am. Soc. Mech. Eng. Press. Vessel. Pip. Div. PVP, 2014. doi:10.1115/PVP2014-28663.